Structural, electronic, and magnetic properties of the possible pnictide superconductor $BaFeAs_2$

Zisheng Gong,[1] Jinyu Zou,[1,*] and Gang Xu[1,2,3,†]

[1] *Wuhan National High Magnetic Field Center and School of Physics, Huazhong University of Science and Technology, Wuhan 430074, China*

[2] *Institute for Quantum Science and Engineering, Huazhong University of Science and Technology, Wuhan 430074, China*

[3] *Wuhan Institute of Quantum Technology, Wuhan 430074, China*

(Received 27 December 2023; revised 9 June 2024; accepted 21 June 2024; published 12 August 2024)

Iron-based superconductors have sparked a large amount of research, but the comprehensive studies on the 112 family are still lacking. $BaFeAs_2$ has been predicted as a promising candidate of an iron-based superconductor. Here we systematically study its stability, electronic structures, and magnetic orders from the first-principles calculations. According to the stacking manners and As distortion in the $[Ba_2As_2]$ layer, four possible $BaFeAs_2$ structures with $P4/nmm$, $P2_1/m$, $I4/mmm$, and $I2mm$ symmetry are constructed. The calculations demonstrate that the most stable structure is determined to be $I2mm$ symmetry, with the structure and valence state in $[Fe_2As_2]$ layers closely resembling the characteristics of iron-based superconductors, as well as the electronic properties and stripe antiferromagnetic ground state. These findings are helpful for further research and comprehensive understanding of the 112-type iron-based superconductors.

DOI: 10.1103/PhysRevB.110.085128

I. INTRODUCTION

The discovery of $LaFeAsO_{1-x}F_x$ with high superconducting transition temperature (T_c) attracts enormous interest in iron-based superconductors [1–3]. Up to now, iron-based superconductors have been realized in multiple prototypical structures, mainly including the 1111 family with the highest $T_c = 55$ K in SmFeAsO [4,5], the 122 family AFe_2As_2 with $A =$ Ca, Sr, or Ba, and T_c around 38 K [6], the 111 family LiFeAs with $T_c = 18$ K [7,8], and the 11 family FeSe with T_c achieving 65 K in its monolayer film [9,10]. These parent compounds of iron-based superconductors are all of similar basic fluorite-type $[Fe_2Pn_2]$ layer, with a square lattice of Fe layer surrounded by the Pn tetrahedron (Pn = P, As, Sb, and Se). The quasi-two-dimensional $[Fe_2Pn_2]$ is mostly separated by the space layers, e.g., $[La_2O_2]$, and can obtain electrons from the space layers to ensure a similar chemical filling and electronic structures, which leads the similar quasi-two-dimensional Fermi surfaces (FSs) with several holes FSs around the Γ point and electron FSs around the M point. Moreover, most parent compounds of the iron-based superconductors form a long-range stripe antiferromagnetic (SAFM) order at low temperatures due to the spin density wave instability, which can be suppressed to realize the superconductivity by electron or hole doping. These commonalities have become important evidence for the exploration of new higher T_c iron-based superconductors theoretically and experimentally.

One usual way to explore new iron-based superconductors is to replace the space layer with other atoms or structural units. The $BaFeAs_2$ (named the 112 family) is first predicted by replacing the $[La_2O_2]$ layer in the LaOFeAs with the $[Ba_2As_2]$ layer as shown by the green rectangle in Fig. 1(a), which owns the same space group $P4/nmm$ as LaOFeAs [11]. Shim *et al.* report that the $[Fe_2As_2]$ layer in $P4/nmm$ $BaFeAs_2$ gives rise to similar electronic structures to other parent compounds of iron-based superconductors, but the $[Ba_2As_2]$ layer will contribute some strong dispersive bands and additional FSs near the X point. In 2013, Yakita *et al.* found T_c around 20 K and 45 K in the rare earth doped monoclinic (Ca, Pr)$FeAs_2$ and $Ca_{1-x}La_xFeAs_2$ with $P2_1$ (No. 4) and $P2_1/m$ (No. 11) symmetry, respectively [12–18]. Such monoclinic phases have a similar structure to the $P4/nmm$ $BaFeAs_2$, except that the zigzag distortion occurs in the As square net of the $[Ba_2As_2]$ layer as shown in Figs. 1(b) and 1(d). Moreover, Kang *et al.* report that $BaFeAs_2$ may adopt the stable $I2mm$ structure as shown in Fig. 1(h) by structural search method, which can be obtained by the $I4/mmm$ $BaMnSb_2$ [see Fig. 1(g)] with a zigzag distorted As net [19–24]. We note that the main difference between $P4/nmm$ ($P2_1/m$) and $I4/mmm$ ($I2mm$) structure is the staking manners of the $[Ba_2Fe_2As_4]$ unit as marked by red and blue rectangles in Figs. 1(a), 1(b) and Figs. 1(g), 1(h). It is clear that the $[Ba_2Fe_2As_4]$ units are stacked directly along the c axis in $P4/nmm$ or $P2_1/m$ structure (named as AA stacking below), while there is a (0.5, 0.5, 0) translation between two adjacent $[Ba_2Fe_2As_4]$ units in Figs. 1(g), 1(h) (named as AB stacking below). As a result, different stacking leads to different $[Ba_2As_2]$ configurations. As marked by the green rectangles in Figs. 1(a), 1(b) and Figs. 1(g), 1(h), the Ba atoms in AA stacking crystals are staggered on both sides of the As net with a PbO-type structure, while the Ba atoms in AB stacking crystals face opposite each other across the As net. The different stacking manners and the As net distortion portend different stability and electronic properties for $BaFeAs_2$. The comprehensive studies on their stability, electronic structures, and magnetic order play

*Contact author: jyzou@hust.edu.cn

†Contact author: gangxu@hust.edu.cn

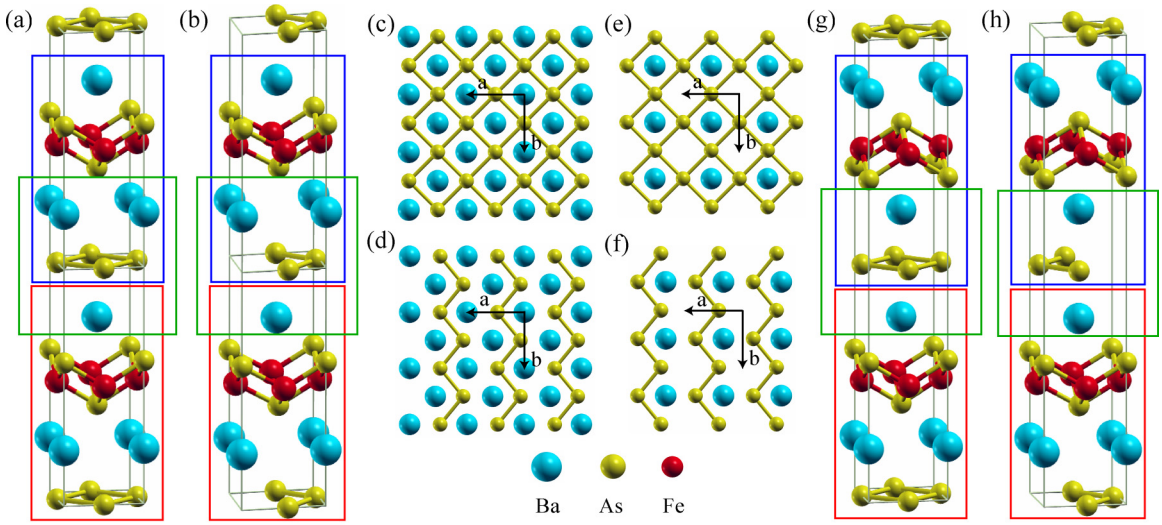

FIG. 1. Crystal structures of $BaFeAs_2$ with (a) $P4/nmm$, (b) $P2_1/m$, (g) $I4/mmm$, and (h) $I2mm$ symmetry. The top view of $[Ba_2As_2]$ layer with (c) $P4/nmm$, (d) $P2_1/m$, (e) $I4/mmm$, and (f) $I2mm$ symmetry. The Ba, Fe, and As atoms are denoted by blue, red, and yellow spheres, respectively. The red and blue rectangles represent $[Ba_2Fe_2As_4]$ units and the green rectangles represent the space layer. The structural distortion occurs in all structures that are fully optimized by DFT.

important roles in understanding the physical properties of the 112 family including the mechanism of their superconductivity, but are still lacking now.

In this paper, we systematically study the stability, electronic structures and magnetic orders of four $BaFeAs_2$ structures with $P4/nmm$, $P2_1/m$, $I4/mmm$, and $I2mm$ symmetry from the first-principles calculations. The density of states (DOS), band structures, and FSs show that the $[Fe_2As_2]$ layer is similar to other parent compounds of iron-based superconductors. The stacking manners and As distortion significantly influence the electronic structures of the $[Ba_2As_2]$ layer. The As square net exhibits some Dirac-type bands near the Fermi level, resulting in several discontinuous diamond-shaped FSs in $P4/nmm$ and $I4/mmm$ structures. Our thermodynamic and dynamic calculation found that the $I2mm$ structure is the most stable one, in which the Dirac-type dispersion is broken by zigzag As distortion, making the corresponding FSs disappear. In addition, the magnetic orders are identified to be stripe antiferromagnetic, similar to other parent compounds of iron-based superconductors.

II. COMPUTATIONAL DETAILS

The Vienna *ab initio* simulation package (VASP) is used for performing the first-principles calculations based on density functional theory (DFT) [25–28]. The generalized-gradient approximation of Perdew, Burke, and Ernzerhof (PBE) is employed to treat the exchange-correlation potential [29]. In this work, the cutoff energy of the plane wave basis is set as 520 eV. Throughout the primitive cell of the Brillouin zone, the Γ-centered k meshes are sampled as $9\times9\times3$ in $P4/nmm$ and $P2_1/m$ structures and the $I4/mmm$ and $I2mm$ structures are sampled as $12\times12\times12$. Structures are fully optimized until the maximum ionic forces are below a threshold of 0.001 eV/Å and electronic self-consistent calculations are within 10^{-6} eV per unit cell. The analysis of the lattice dynamics of all structures is done by PHONOPY based on the Parlinsk-Li-Kawasoe method [30]. We also performed DFT+U calculations and found that the Coulomb correlation brings nearly no influence to the spatial, electronic, and magnetic structure of $BaFeAs_2$ (see Appendix A for detail). This agrees with the previous literature [31–34] that the DFT results based on the nonmagnetic structure in iron-based superconductors fit the angle-resolved photoemission spectroscopy (ARPES) measurements very well. Hence we concentrate on the DFT results based on nonmagnetic structure in the following and disregard the impact of different magnetic configurations on the structure.

III. RESULTS AND DISCUSSION

A. Structures and stability

As introduced above, four crystal structures of $BaFeAs_2$ with $P4/nmm$ [Fig. 1(a)], $P2_1/m$ [Fig. 1(b)], $I4/mmm$ [Fig. 1(g)], and $I2mm$ [Fig. 1(h)] symmetry are constructed and the fully optimized parameters are summarized in Table I, where As atoms are named As1 in the $[Ba_2As_2]$ layer and As2 in the $[Fe_2As_2]$ layer. It is worth noticing that the changes of the $[Fe_2As_2]$ layers in four structures, including the Fe-Fe length and Fe-As2 length, are very weak after the optimization, as listed in Table I.

The total energy is first calculated to study the stability of four structures. As listed in Table I, the $I2mm$ structure shows the lowest total energy in $BaFeAs_2$. Detailed comparison shows that the energy of the zigzag distorted $I2mm$ ($P2_1/m$) structure is 165 meV (175 meV) lower than that of the undistorted $I4/mmm$ ($P4/nmm$) structure. The energy reduction caused by the zigzag distortion of the As1 net can be interpreted as the Peierls instability [35], which commonly occurs in the square net of the group VA elements and tends to dimerize the square net to form the stable chains, just as reported in the isomorphic compounds $SmAuAs_2$ [36], $CaFeAs_2$ [12–14], and $BaMnSb_2$ [23,24]. On the other hand, the $I2mm$ ($I4/mmm$) structure with AB stacking is 16.1 meV

TABLE I. Lattice constants, atom coordinates(fractional), bond lengths of Fe-Fe and Fe-As2, bond angles of As2-Fe-As2, and total energy for $P4/nmm$, $P2_1/m$, $I4/mmm$, and $I2mm$ $BaFeAs_2$.

Parameter	$P4/nmm$	$P2_1/m$	$I4/mmm$	$I2mm$
a (Å)	3.9803	4.0715	3.9861	4.0593
b (Å)	3.9803	3.9789	3.9861	3.9871
c (Å)	11.7260	11.6016	23.3423	23.1719
α, γ, β	$\alpha = \gamma = \beta = 90^\circ$	$\alpha = \beta = 90^\circ, \gamma = 91.4504^\circ$	$\alpha = \gamma = \beta = 90^\circ$	$\alpha = \gamma = \beta = 90^\circ$
Ba	2c (0.2500, 0.2500, 0.2334)	2e (0.7331, 0.2500, 0.2353)	4e (0.0000, 0.0000, 0.1157)	4d (0.0084, 0.0000, 0.1168)
Fe	2b (0.7500, 0.2500, 0.5000)	2e (0.2499, 0.2500, 0.5015)	4d (0.0000, 0.5000, 0.2500)	4d (0.2505, 0.0000, 0.5098)
As1	2a (0.7500, 0.2500, 0.0000)	2e (0.2427, 0.7500, 0.3962)	4c (0.0000, 0.5000, 0.0000)	2a (0.0217, 0.5000, 0.5000) 2b (0.4224, 0.0000, 0.5000)
As2	2c (0.2500, 0.2500, 0.6048)	2e (0.2000, 0.7500, 0.0039)	4e (0.0000, 0.0000, 0.6975)	4d (0.0099, 0, 0.6980)
Fe-Fe (Å)	2.8145	2.8478/2.8455	2.8186	2.8450
Fe-As2 (Å)	2.3392	2.3561/2.3339	2.3396	2.3540/2.3361
As2-Fe-As2 (°)	116.5912	119.5286/116.9558	116.8311	119.1013/117.1603
Energy (eV)	−43.6388	−43.8139	−43.6653	−43.8300

(26.5 meV) lower than that of the $P2_1/m$ ($P4/nmm$) structure with AA stacking. The reason for lower energy in AB stacking may be that the oppositely placed Ba ions weaken the dipole interactions between adjacent dipoles in AA stacking [37–39]. Different ions and pressure may lead to different structures. Appendix B further investigates the ground state structure stability of $BaFeAs_2$ under various pressures, revealing that the ground state transitions from $I2mm$ to the $P2_1/m$ structure under in-plane stress.

The dynamic stability of these structures is further checked by phonon spectrum calculations. As shown in Fig. 2, there are two negative optical phonons in $P4/nmm$ and $I4/mmm$ structures, while the two negative optical phonons disappear in $P2_1/m$ and $I2mm$ structures. It manifests that the two negative optical phonons are originated from the instability of the As1 square net, consistent with the study of total energy. Furthermore, the $P2_1/m$ structure and $I2mm$ structure in different stacking manners are dynamically stable, indicating that the different stacking manners have little effect on dynamic instability. All these results demonstrate that the $I2mm$ $BaFeAs_2$ is stable thermodynamically and dynamically.

To investigate the chemical bonding properties, the differential charge density of $I2mm$ $BaFeAs_2$ is calculated using the following formula:

$$\Delta\rho = \rho_{BaFeAs_2} - \rho_{Ba} - \rho_{Fe} - \rho_{As}. \quad (1)$$

As shown in the distribution in Fig. 3, the green regions have little change in charge density and the red regions represent the charge accumulation and form the chemical bond. As shown in Fig. 3(a), the green regions on both sides of the $[Fe_2As_2]$ layer ensure their quasi-two-dimensional property and the strong charge density accumulation along the Fe-As2 direction demonstrates that Fe atoms and As2 atoms are strongly bonded to form the stable $[Fe_2As_2]$. As a result, the differential charge distribution on the [001] plane of Fe and As2, as plotted in Figs. 3(b) and 3(c), exhibits similar

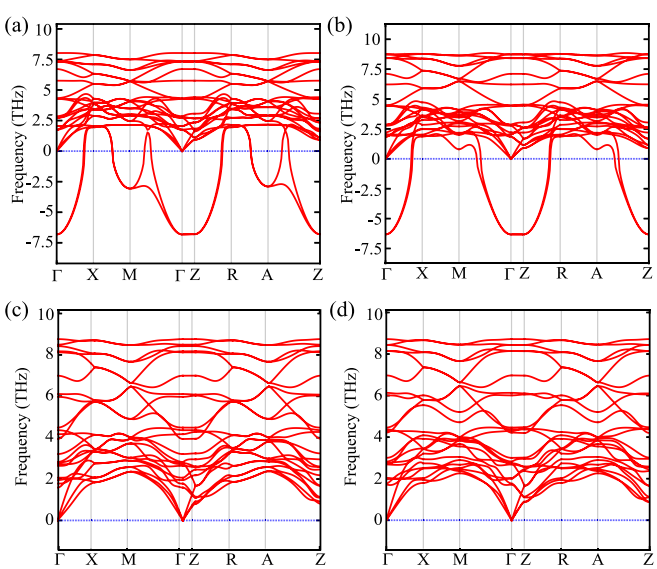

FIG. 2. Phonon spectrum of $BaFeAs_2$ with (a) $P4/nmm$, (b) $I4/mmm$, (c) $P2_1/m$, and (d) $I2mm$ symmetry.

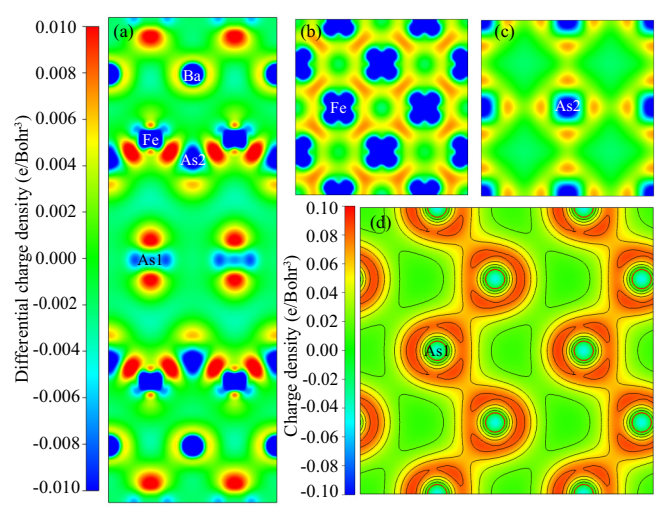

FIG. 3. Differential charge density on (a) [100] plane, (b) [001] plane of Fe layer, and (c) [001] plane of As2 layer in $I2mm$ $BaFeAs_2$. (d) The charge density on the [001] plane of As1 layer in $I2mm$ $BaFeAs_2$.

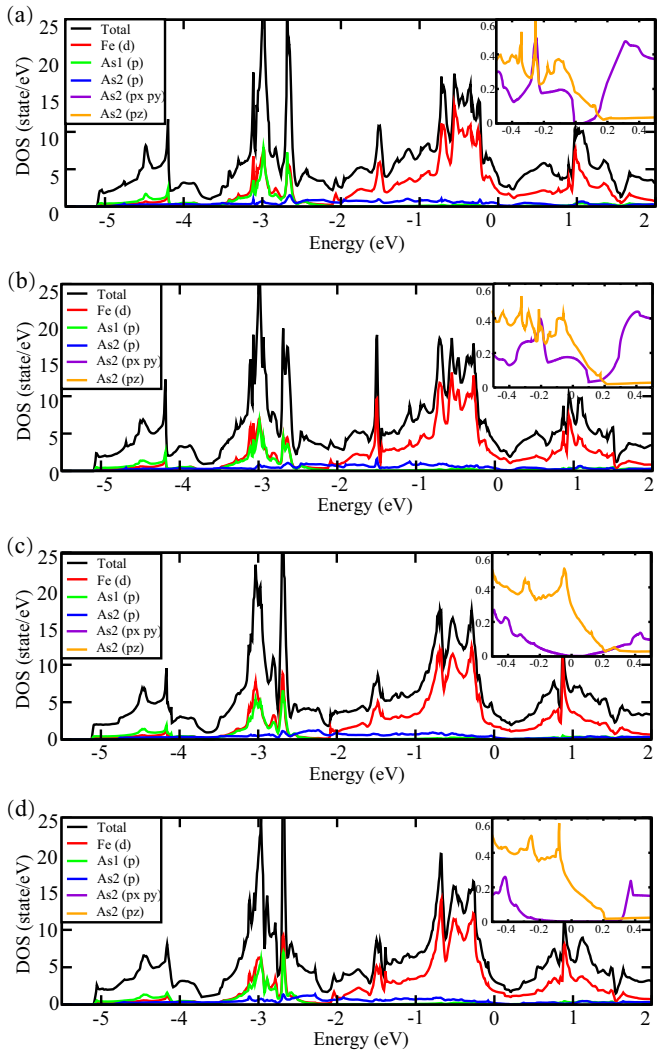

FIG. 4. Total and projected DOS of $BaFeAs_2$ with (a) $P4/nmm$, (b) $I4/mmm$, (c) $P2_1/m$, and (d) $I2mm$ symmetry. The inset figures display the corresponding p_x/p_y and p_z orbitals of As1 near the Fermi level.

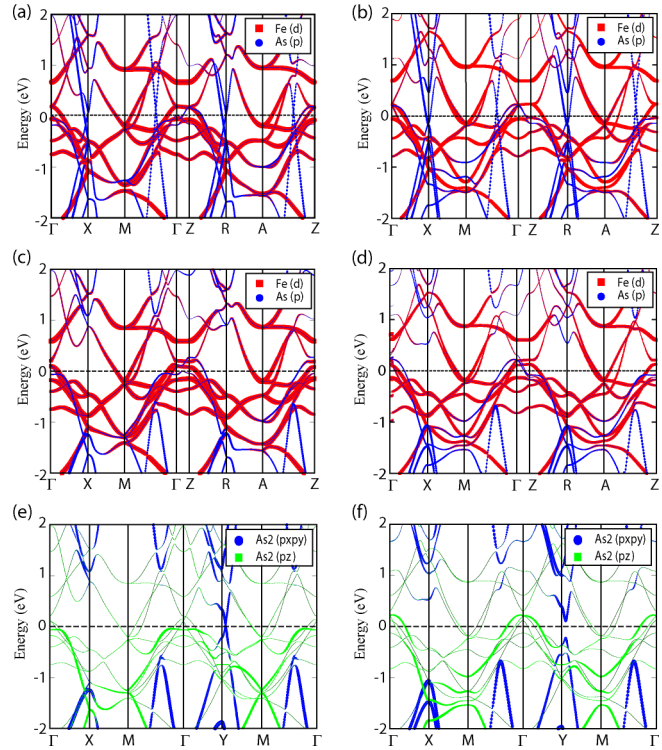

FIG. 5. Projected bands of $BaFeAs_2$ with (a) $P4/nmm$, (b) $I4/mmm$, (c) $P2_1/m$, and (d) $I2mm$ symmetry. The red square and blue circle represent the $3d$ orbitals of Fe and the $4p$ orbitals of As, respectively. The projected bands of As1 orbitals with (e) $P2_1/m$ and (f) $I2mm$ symmetry in distorted (X) and undistorted (Y) direction. The blue circle and green square represent the p_x/p_y orbital of As1 and p_z orbital of As, respectively.

bonding properties to the $[Fe_2As_2]$ layer in other parent compounds of iron-based superconductors [40,41]. Thus the Fe and As2 ions are inferred to be +2 and −3 valence, respectively, where $As2^{3-}$ receives two electrons from Fe^{2+} and one electron from Ba^{2+}. In addition, the charge aggregation on the p_z orbital of As1, as shown in Fig. 3(a), indicates that the Ba^{2+} ions contribute another electron to the p_z orbital of As1. Therefore, the As1 ions exhibit −1 valence and their half-full p_x and p_y orbitals are going to form covalent bonds with the adjacent As1 atoms. Such covalent bonds usually tend to form a zigzag-shaped distortion to lower the total energy, as shown in Fig. 3(d) [42].

B. Electronic structure

In this section, we discuss the electronic structures of four kinds of crystal structures, including their DOS, band structures, and FSs. Figure 4 shows that the total and projected DOS (PDOS) of four structures exhibit similar shapes. The $3d$ orbitals of Fe dominate the total DOS near the Fermi level from −2 eV to 2 eV and a pseudogap of about 0.5 eV appears slightly above the Fermi level. The $3p$ orbitals of As2 are predominantly distributed in the occupied state from −3.5 eV to −2.5 eV and are considerably hybridized with the $3d$ orbitals of Fe. These features are consistent with the DOS observed in other parent compounds of iron-based superconductors, indicating similar bonding structures in the $[Fe_2As_2]$ layer. However, the As1 atoms in four structures are in contrary to the insulating $[La_2O_2]$ layer of LaOFeAs, exhibiting an extensive energy distribution in PDOS. While the p_z orbital of As1 exhibits almost the same metallic properties in four structures, the p_x/p_y orbital is distinct, as shown by the orange (p_z) and purple (p_x/p_y) lines in the inset of Fig. 4. Compared with the case in the As1 square net, the zigzag distorted As1 net leads to a noticeable decrease of the p_x/p_y orbital near the Fermi level, as shown in the insets of Figs. 4(c) and 4(d), with an energy gap of about 0.4 eV in AB stacking.

The projected band structures of Fe and As orbitals can further reveal such features. As shown by the red square in Figs. 5(a)–5(d), the $3d$ orbitals of Fe atoms form two electron-type pockets near the M and A points and two hole-type pockets near the Γ and Z points. The band dispersion along the Γ-Z path is very weak, revealing the quasi-two-dimensional feature of $[Fe_2As_2]$. These

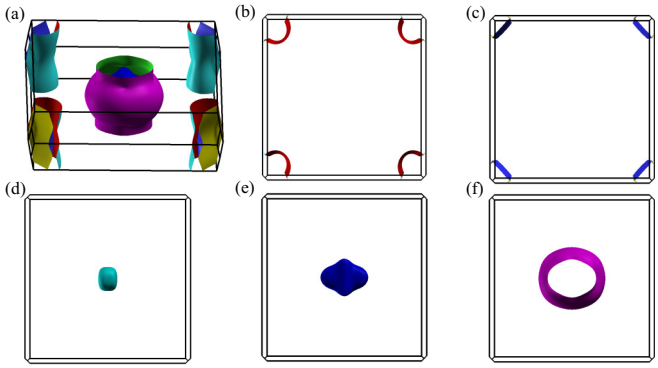

FIG. 6. Total FSs and individual FSs for $I2mm$ $BaFeAs_2$.

properties are consistent with previous research on parent compounds of iron-based superconductors.

In contrast, the bands of space layer for four structures behave distinctly. The $4p$ orbitals of As1 exhibit numerous Dirac-type dispersion near the Fermi level before the zigzag distortion, as indicated by the blue circle in Figs. 5(a) and 5(b). These band structures cross the Fermi level leading to several discontinuous diamond-shaped FSs connecting X points, as analyzed in Ref. [15]. With the zigzag distortion, the Dirac-type dispersions are destroyed with a band gap of at least 1 eV in the distorted direction (a axis), as shown near the X and R points in Figs. 5(c) and 5(d). In the undistorted direction (b axis), the Dirac-type dispersion is preserved in AA stacking, while a band gap of 0.4 eV is opened in AB stacking, as shown by the blue points in Figs. 5(e) and 5(f). These different band dispersions contributed by the $[Ba_2As_2]$ layer give rise to different FSs.

The FSs of the stable $I2mm$ $BaFeAs_2$ are shown in Fig. 6, with three hole-type FSs around Γ points and two electron-type FSs along the M-R path. These FSs are mainly contributed by the $[Fe_2As_2]$ layer, with the exception of the FS shown in Fig. 6(f), where significant hybridization of p_z orbitals of As1 occurs [refer to Fig. 5(f)]. It suggests the occurrence of self-doping through charge transfer between $[Ba_2As_2]$ and $[Fe_2As_2]$. Such FS exhibit moderate dispersion along the Γ-Z direction, probably caused by the p_z orbital of As1, which weakens the quasi-two-dimensional properties in $BaFeAs_2$. It is obvious that the fully gapped p_x/p_y orbitals of As1 in the $I2mm$ structure do not contribute any FSs in the Brillouin zone, different from the FSs in $BaFeAs_2$ before zigzag distortion. Furthermore, due to the breaking of fourfold rotation (C_{4z}) symmetry in the zigzag distorted As1 net, the FSs are no longer symmetric between the distorted and undistorted directions, as manifested by Fig. 6(e) and Fig. 6(f).

TABLE II. Total energy of four structures for $BaFeAs_2$ in three magnetic orders (NM, CAFM, and SAFM).

Energy	$P4/nmm$	$P2_1/m$	$I4/mmm$	$I2mm$
NM (eV/f.u.)	−43.6388	−43.8139	−43.6653	−43.8300
CAFM (eV/f.u.)	−43.6694	−43.8509	−43.6964	−43.8668
SAFM (eV/f.u.)	−43.7350	−43.9249	−43.7675	−43.9459
J_1 (meV/f.u.)	31.70	37.00	33.32	38.18
J_2 (meV/f.u.)	24.05	27.75	25.55	28.98

C. Magnetic properties

Conventionally, iron-based superconductors exhibit spin density wave in their parent phase, implying the important role of magnetic order in iron-based superconductors. The total energy of four structures with nonmagnetic (NM), checkboard antiferromagnetic (CAFM), and SAFM configurations are displayed in Table II (all four magnetic configurations are based on the same structure as the NM configurations). The ferromagnetic (FM) order is found to be unstable and the energy is converging to the NM state. Similar to most iron-based superconducting parent materials, the SAFM state is the ground state for all the structures with an energy advantage of about 100 meV/70 meV over the NM/CAFM state, and is minorly affected by the stacking manners and distortion.

The exchange interaction strength is also calculated. The J_1-J_2 model is widely used to assess various possible ordered states in iron-based superconductors, where J_1 is the nearest-neighbor exchange coupling and J_2 is the next-nearest-neighbor exchange coupling. According to mean-field theory, the energy per Fe of CAFM can be expressed as $E_1 = -2J_1 + 2J_2$ and the total energy is $2E_1$. Energy per Fe of SAFM can be expressed as $E_2 = -2J_2$ and total energy is $2E_2$. Therefore, when $J_2 > J_1/2$, the next-nearest-neighbor exchange coupling dominates, leading to a SAFM order in the system. As shown in Table II, all four structures satisfy

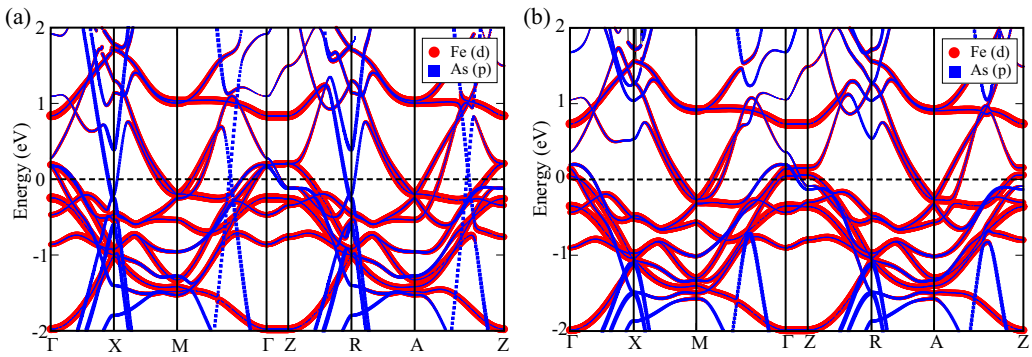

FIG. 7. DFT+U method calculated projected bands of $BaFeAs_2$ with (a) $I4/mmm$ and (b) $I2mm$ symmetry. The red square and blue circle represent the $3d$ orbitals of Fe and the $4p$ orbitals of As, respectively.

TABLE III. Total energy of four $BaFeAs_2$ in four magnetic orders (NM, FM, CAFM, and SAFM). Each magnetic order structure is optimized and the parameter of DFT+U is $U = 2.5$ eV and $J = 0.2$ eV.

Energy (eV/f.u.)	$P4/nmm$	$P2_1/m$	$I4/mmm$	$I2mm$
NM	−38.4811	−38.6578	−38.5065	−38.6742
FM	−39.9225	−40.1648	−39.9425	−40.1750
CAFM	−40.1227	−40.3574	−40.1816	−40.3679
SAFM	−40.4723	−40.7330	−40.5665	−40.7564

$J_2 > J_1/2$, indicating that the magnetic ground state of all these structures is of SAFM order. This is consistent with observations in parent compounds of iron-based superconductors, particularly $BaFe_2As_2$ [43].

IV. SUMMARY

To summarize, we construct four possible $BaFeAs_2$ structures to study the 112 family iron-based superconductor. The calculated results reveal that $I2mm$ structure with AB stacking and zigzag distorted As1 net is the most stable one. Comparing to square As1 net, the zigzag distortion opens the gap in the Dirac-type bands and thus erases the discontinuous diamond-shaped FSs. Additionally, the magnetic ground states of $I2mm$ $BaFeAs_2$ exhibit SAFM order. These properties exhibit great similarities to most parent compounds of iron based superconductors, indicating the $I2mm$ $BaFeAs_2$ to be the parent compound of the 112 family. Hence the further experimental exploration of this parent compound is meaningful. Considering the self-doping effect between As1 and Fe atoms, the superconductivity is strongly expected. Otherwise, alternative explanations should be proposed to complement the understanding of iron-based superconductivity.

ACKNOWLEDGMENTS

This work is supported by the National Natural Science Foundation of China (Grant No. 12274154). The computation is completed in the HPC Platform of Huazhong University of Science and Technology.

TABLE IV. Lattice constants (a, b, and c) of four $BaFeAs_2$ in three magnetic orders (NM, CAFM, and SAFM). Each magnetic order structure is optimized and the parameter of DFT+U is $U = 2.5$ eV and $J = 0.2$ eV.

Parameter (Å)	$P4/nmm$	$P2_1/m$	$I4/mmm$	$I2mm$
a_{NM}	3.9811	4.0747	3.9860	4.0669
b_{NM}	3.9811	3.9807	3.9860	3.9922
c_{NM}	11.6862	11.5562	23.2742	23.0361
a_{CAFM}	4.1126	4.3087	4.1151	4.2163
b_{CAFM}	4.1126	4.0665	4.1151	4.1108
c_{CAFM}	11.7968	11.6167	23.5068	23.2715
a_{SAFM}	4.1034	4.2196	4.0926	4.1652
b_{SAFM}	4.1034	4.0772	4.0926	4.0985
c_{SAFM}	11.8649	11.7466	23.7131	23.5192

TABLE V. Total energy of four $BaFeAs_2$ in different hydrostatic pressure.

Energy (eV/f.u.)	$P4/nmm$	$P2_1/m$	$I4/mmm$	$I2mm$
−10 Gpa	−43.6383	−43.8131	−43.6631	−43.8295
0 GPa	−43.6388	−43.8139	−43.6653	−43.8300
10 Gpa	−32.7650	−32.8428	−32.8103	−32.8835
20 GPa	−22.9096	−22.9411	−22.9776	−22.9780
30 GPa	−13.7277	−13.7277	−13.8202	−13.8202

APPENDIX A: INFLUENCE OF CORRELATION AND MAGNETIC STRUCTURE ON THE ELECTRONIC, SPATIAL, AND MAGNETIC PROPERTIES OF $BaFeAs_2$

The DFT+U method is calculated to see the influence of the electron correlation effect. We apply $U = 2.5$ eV and Hund's coupling $J = 0.2$ eV, and show the projected bands in Fig. 7, the total energy in Table III, and the optimized lattice constant in Table IV [44,45]. Comparing to the results in Figs. 5(b) and 5(d) of the main text, the bands near the Fermi level remain unchanged. The structural and magnetic ground states remain in $I2mm$ and SAFM. The lattice constants considering DFT+U (the nonmagnetic state in Table IV) show only about a 0.02% variation compared to the DFT results (Table I in the main text).

In addition, we use the DFT+U method to optimize the structure of each magnetic state and check its influence on spatial structure, as shown in Tables III and IV. An increase of the lattice constants by approximately 4% can be observed as the result of the relaxation of the magnetic configuration. Nevertheless, the magnetic ground state of each structure remains in the $I2mm$ structure.

APPENDIX B: STRESS INDUCED POSSIBLE PHASE TRANSITION FROM $I2mm$ to $P2_1/m$

To see the possible transition of the ground state structure in $BaFeAs_2$ under stresses, hydrostatic pressure and uniaxial strain are applied in this section. While the hydrostatic pressure from −10 GPa to 30 GPa is applied to find the possible structural phase transition in $BaFeAs_2$, it remains in the $I2mm$ phase (see Table V). At 30 GPa, the zigzag distorted As2 converge to the square net. Further tests involving compression or stretch along the c axis up to 10% showed no trend of phase transition. Nevertheless, when the ab axis was compressed to 10%, the $P2_1/m$ structure became the ground state, as shown in Table VI. Thus increasing pressure along the in-plane ab direction can induce the structural transition from $I2mm$ to $P2_1/m$.

TABLE VI. Total energy of four $BaFeAs_2$ in different in-plane strains.

Energy (eV/f.u.)	$P4/nmm$	$P2_1/m$	$I4/mmm$	$I2mm$
ab-2%	−43.5865	−43.7682	−43.6125	−43.7837
ab-5%	−43.2666	−43.4864	−43.2976	−43.5004
ab-8%	−42.5905	−42.8959	−42.6262	−42.9006
ab-10%	−41.9049	−42.3042	−41.8951	−42.2955

[1] D. N. Basov and A. V. Chubukov, Manifesto for a higher T_c, Nat. Phys. **7**, 272 (2011).

[2] G. R. Stewart, Superconductivity in iron compounds, Rev. Mod. Phys. **83**, 1589 (2011).

[3] P. J. Hirschfeld, M. M. Korshunov, and I. I. Mazin, Gap symmetry and structure of Fe-based superconductors, Rep. Prog. Phys. **74**, 124508 (2011).

[4] R. Zhi-An, L. Wei, Y. Jie, Y. Wei, S. Xiao-Li, Zheng-Cai, C. Guang-Can, D. Xiao-Li, S. Li-Ling, Z. Fang, and Z. Zhong-Xian, Superconductivity at 55 K in iron-based F-doped layered quaternary compound $Sm[O_{1-x}F_x]$ FeAs, Chin. Phys. Lett. **25**, 2215 (2008).

[5] C. Wang, L. Li, S. Chi, Z. Zhu, Z. Ren, Y. Li, Y. Wang, X. Lin, Y. Luo, S. Jiang, X. Xu, G. Cao, and Z. Xu, Thorium-doping–induced superconductivity up to 56 K in $Gd_{1-x}Th_x$ FeAsO, Europhys. Lett. **83**, 67006 (2008).

[6] M. Rotter, M. Tegel, and D. Johrendt, Superconductivity at 38 K in the iron arsenide $(Ba_{1-x}K_x)Fe_2As_2$, Phys. Rev. Lett. **101**, 107006 (2008).

[7] X. C. Wang, Q. Q. Liu, Y. X. Lv, W. B. Gao, L. X. Yang, R. C. Yu, F. Y. Li, and C. Q. Jin, The superconductivity at 18 K in LiFeAs system, Solid State Commun. **148**, 538 (2008).

[8] C. W. Chu, F. Chen, M. Gooch, A. M. Guloy, B. Lorenz, B. Lv, K. Sasmal, Z. J. Tang, J. H. Tapp, and Y. Y. Xue, The synthesis and characterization of LiFeAs and NaFeAs, Physica C: Supercond. **469**, 326 (2009).

[9] J.-F. Ge, Z.-L. Liu, C. Liu, C.-L. Gao, D. Qian, Q.-K. Xue, Y. Liu, and J.-F. Jia, Superconductivity above 100 K in single-layer FeSe films on doped $SrTiO_3$, Nat. Mater. **14**, 285 (2015).

[10] Z.-C. Zhang, Y.-H. Wang, Q. Song, C. Liu, R. Peng, K. A. Moler, D.-L. Feng, and Y.-Y. Wang, Onset of the meissner effect at 65 K in FeSe thin film grown on Nb-doped $SrTiO_3$ substrate, Sci. Bull. **60**, 1301 (2015).

[11] J. H. Shim, K. Haule, and G. Kotliar, Density-functional calculations of the electronic structures and magnetism of the pnictide superconductors $BaFeAs_2$ and $BaFeSb_2$, Phys. Rev. B **79**, 060501(R) (2009).

[12] A. Sala, H. Yakita, H. Ogino, T. Okada, A. Yamamoto, K. Kishio, S. Ishida, A. Iyo, H. Eisaki, M. Fujioka, Y. Takano, M. Putti, and J. Shimoyama, Synthesis and physical properties of $Ca_{1-x}RE_xFeAs_2$ with RE= La–Gd, Appl. Phys. Express **7**, 073102 (2014).

[13] S. Jiang, C. Liu, H. Cao, T. Birol, J. M. Allred, W. Tian, L. Liu, K. Cho, M. J. Krogstad, J. Ma, K. M. Taddei, M. A. Tanatar, M. Hoesch, R. Prozorov, S. Rosenkranz, Y. J. Uemura, G. Kotliar, and N. Ni, Structural and magnetic phase transitions in $Ca_{0.73}La_{0.27}FeAs_2$ with electron-overdoped FeAs layers, Phys. Rev. B **93**, 054522 (2016).

[14] H. Yakita, H. Ogino, T. Okada, A. Yamamoto, K. Kishio, T. Tohei, Y. Ikuhara, Y. Gotoh, H. Fujihisa, K. Kataoka *et al.*, A new layered iron arsenide superconductor:(Ca, Pr) $FeAs_2$, J. Am. Chem. Soc. **136**, 846 (2014).

[15] N. Katayama, K. Kudo, S. Onari, T. Mizukami, K. Sugawara, Y. Sugiyama, Y. Kitahama, K. Iba, K. Fujimura, N. Nishimoto *et al.*, Superconductivity in $Ca_{1-x}La_xFeAs_2$: A novel 112-type iron pnictide with arsenic zigzag bonds, J. Phys. Soc. Jpn. **82**, 123702 (2013).

[16] Y.-N. Huang, X.-L. Yu, D.-Y. Liu, and L.-J. Zou, Magnetism and electronic structures of novel layered $CaFeAs_2$ and $Ca_{0.75}(Pr/La)_{0.25}FeAs_2$, J. Appl. Phys. **117**, 17E113 (2015).

[17] J. Yu, T. Liu, B.-J. Pan, B.-B. Ruan, X.-C. Wang, Q.-G. Mu, K. Zhao, G.-F. Chen, and Z.-A. Ren, Discovery of a novel 112-type iron-pnictide and La-doping induced superconductivity in $Eu_{1-x}La_xFeAs_2$ (x=0–0.15), Sci. Bull. **62**, 218 (2017).

[18] M. Y. Li, Z. T. Liu, W. Zhou, H. F. Yang, D. W. Shen, W. Li, J. Jiang, X. H. Niu, B. P. Xie, Y. Sun, C. C. Fan, Q. Yao, J. S. Liu, Z. X. Shi, and X. M. Xie, Significant contribution of as $4p$ orbitals to the low-lying electronic structure of the 112-type iron-based superconductor $Ca_{0.9}La_{0.1}FeAs_2$, Phys. Rev. B **91**, 045112 (2015).

[19] C.-J. Kang, T. Birol, and G. Kotliar, Phase stability and large in-plane resistivity anisotropy in the 112-type iron-based superconductor $Ca_{1-x}La_xFeAs_2$, Phys. Rev. B **95**, 014511 (2017).

[20] J. Liu, J. Hu, H. Cao, Y. Zhu, A. Chuang, D. Graf, D. Adams, S. Radmanesh, L. Spinu, I. Chiorescu *et al.*, Nearly massless dirac fermions hosted by Sb square net in $BaMnSb_2$, Sci. Rep. **6**, 30525 (2016).

[21] G. Cordier and H. Schäfer, Darstellung und kristallstruktur von $BaMnSb_2$, $SrMnBi_2$ und $BaMnBi_2$/preparation and crystal structure of $BaMnSb_2$, $SrMnBi_2$ and $BaMnBi_2$, Z. Naturforsch. B **32**, 383 (1977).

[22] J. K. Wang, L. L. Zhao, Q. Yin, G. Kotliar, M. S. Kim, M. C. Aronson, and E. Morosan, Layered transition-metal pnictide $SrMnBi_2$ with metallic blocking layer, Phys. Rev. B **84**, 064428 (2011).

[23] J. Y. Liu, J. Yu, J. L. Ning, H. M. Yi, L. Miao, L. J. Min, Y. F. Zhaos *et al.*, Spin-valley locking and bulk quantum Hall effect in a noncentrosymmetric dirac semimetal $BaMnSb_2$, Nat. Commun. **12**, 4062 (2021).

[24] H. Sakai, H. Fujimura, S. Sakuragi, M. Ochi, R. Kurihara, A. Miyake, M. Tokunaga, T. Kojima, D. Hashizume, T. Muro, K. Kuroda, T. Kondo, T. Kida, M. Hagiwara, K. Kuroki, M. Kondo, K. Tsuruda, H. Murakawa, and N. Hanasaki, Bulk quantum Hall effect of spin-valley coupled dirac fermions in the polar antiferromagnet $bamnsb_2$, Phys. Rev. B **101**, 081104(R) (2020).

[25] P. E. Blöchl, Projector augmented-wave method, Phys. Rev. B **50**, 17953 (1994).

[26] G. Kresse and J. Furthmüller, Efficiency of ab-initio total energy calculations for metals and semiconductors using a plane-wave basis set, Comput. Mater. Sci. **6**, 15 (1996).

[27] G. Kresse and D. Joubert, From ultrasoft pseudopotentials to the projector augmented-wave method, Phys. Rev. B **59**, 1758 (1999).

[28] G. Kresse and J. Furthmüller, Efficient iterative schemes for ab initio total-energy calculations using a plane-wave basis set, Phys. Rev. B **54**, 11169 (1996).

[29] J. P. Perdew, K. Burke, and M. Ernzerhof, Generalized gradient approximation made simple, Phys. Rev. Lett. **77**, 3865 (1996).

[30] A. Togo, F. Oba, and I. Tanaka, First-principles calculations of the ferroelastic transition between rutile-type and $CaCl_2$-type Sio_2 at high pressures, Phys. Rev. B **78**, 134106 (2008).

[31] D. H. Lu, M. Yi, S.-K. Mo, A. S. Erickson, J. Analytis, J.-H. Chu, D. J. Singh, Z. Hussain, T. H. Geballe, I. R. Fisher *et al.*, Electronic structure of the iron-based superconductor LaOFeP, Nature (London) **455**, 81 (2008).

[32] R. P. Day, M. X. Na, M. Zingl, B. Zwartsenberg, M. Michiardi, G. Levy, M. Schneider, D. Wong, P. Dosanjh, T. M. Pedersen, S. Gorovikov, S. Chi, R. Liang, W. N. Hardy, D. A. Bonn, S. Zhdanovich, I. S. Elfimov, and A. Damascelli,

Three-dimensional electronic structure of LiFeAs, Phys. Rev. B **105**, 155142 (2022).

[33] A. Fedorov, A. Yaresko, E. Haubold, Y. Kushnirenko, T. Kim, B. Büchner, S. Aswartham, S. Wurmehl, and S. Borisenko, Energy scale of nematic ordering in the parent iron-based superconductor $BaFe_2As_2$, Phys. Rev. B **100**, 024517 (2019).

[34] R. P. Day, B. Zwartsenberg, I. S. Elfimov, and A. Damascelli, Computational framework chinook for angle-resolved photoemission spectroscopy, npj Quantum Mater. **4**, 54 (2019).

[35] C. Kittel and P. McEuen, *Introduction to Solid State Physics* (John Wiley & Sons, New York, 2018).

[36] K Mukherjee, E. Sampathkumaran, D Rutzinger, T. Doert, and M Ruck, Magnetic and electrical transport anomalies of $RMAs_2$ (R= Pr and Sm, M= Ag and Au), J. Phys.: Condens. Matter **21**, 506004 (2009).

[37] P. V. Balachandran, J. Young, T. Lookman, and J. M. Rondinelli, Learning from data to design functional materials without inversion symmetry, Nat. Commun. **8**, 14282 (2017).

[38] C. P. Brock and J. D. Dunitz, Towards a grammar of crystal packing, Chem. Mater. **6**, 1118 (1994).

[39] S. Haindl, S. Nikolaev, M. Sato, M. Sasase, and I. MacLaren, Engineering of Fe-pnictide heterointerfaces by electrostatic principles, NPG Asia Mater. **13**, 67 (2021).

[40] E. Aktürk and S. Ciraci, First-principles study of the iron pnictide superconductor $BaFe_2As_2$, Phys. Rev. B **79**, 184523 (2009).

[41] F. Ma, W. Ji, J. Hu, Z.-Y. Lu, and T. Xiang, First-principles calculations of the electronic structure of tetragonal α-FeTe and α-FeSe crystals: Evidence for a bicollinear antiferromagnetic order, Phys. Rev. Lett. **102**, 177003 (2009).

[42] M. Eschen and W. Jeitschko, Preparation and crystal structures of ternary rare earth silver and gold arsenides $lnAgAs_2$ and $lnAuAs_2$ with ln = La–Nd, Sm, Gd, and Tb, Z. Naturforschung B **58**, 399 (2003).

[43] G. Xu, H. Zhang, X. Dai, and Z. Fang, Electron-hole asymmetry and quantum critical point in hole-doped $BaFe_2As_2$, Europhys. Lett. **84**, 67015 (2008).

[44] P. Vilmercati, C. P. Cheney, F. Bondino, E. Magnano, M. Malvestuto, M. A. McGuire, A. S. Sefat, B. C. Sales, D. Mandrus, D. J. Singh, M. D. Johannes, and N. Mannella, Direct probe of the variability of Coulomb correlation in iron pnictide superconductors, Phys. Rev. B **85**, 235133 (2012).

[45] E. Bascones, B. Valenzuela, and M. J. Calderón, Magnetic interactions in iron superconductors: A review, C. R. Phys. **17**, 36 (2016).